Effects of nanosilica on the calcium silicate hydrates in Portland cement-fly ash systems

Juliana Calabria-Holley, Kevin Paine and Styliani Papatzani
Department of Architecture and Civil Engineering, University of Bath, United Kingdom

ABSTRACT

Cementitious materials show a complex chemistry and naturally form nanostructures in the hydration process, the network of calcium silicate hydrates (C-S-H). It is considered that nanoparticles such as nanosilica could act as a pozzolanic material as well as a seeding agent for nucleation and acceleration of the formation of calcium silicate hydrates network.

This work evaluates the effect of nanosilica in the C-S-H network and microstructure of the hardened ternary, quaternary and quinary low Portland cement based pastes. The quinary system containing Portland cement, limestone, fly ash, micro and nanosilica and ternary combinations (Portland cement, limestone and fly-ash) show the mean Ca/Si atomic ratio of the C-S-H gel in the 28 day-old hardened paste of 1.2 and 2.3 respectively. FTIR results show the presence of bridging silicate tetraedra (Q^2) characteristic of a peak at around 980 cm^{-1} and by a shoulder at around 1060 cm^{-1} in the C-S-H gel network of the ternary, quaternary and quinary combinations, thus these bands are more pronounced for the nanosilica enhanced formulations. The sample obtained in the presence of micro and nanosilica (quinary combination) showed evidence of a more intricate C-S-H gel network (bringing tetraedra) characteristic of honeycomb-like structure opposed to the ternary combination.

Keywords: C-S-H networking, nanosilica, fly ash

INTRODUCTION

Nano materials have high specific surface area and in general, the greater the specific surface area of the material, the more reactive it is. Nanosilica has a large field of applications ranging from biomaterials such as bone and tissue regeneration (Lenza and Vasconcelos, 2001a; Lenza and Vasconcelos, 2001b) to the semiconductor industry. In recent years the cement industry has also benefited from incorporating nanomaterials such as nanosilica, nanolimestone and nanoclay into mixes (Kawashima *et al.*, 2013; Bentz *et al.*, 2012; Hou *et al*., 2012; Sato *et al.*, 2011; *Raki et al..*, 2010; Tregger *et al*., 2010; Sobolev *et al*., 2009; Bjornstrom *et al.*, 2004). The addition of nanosilica has been reported to improve the strength gain, resistance to sulfate attack, and alkali-silica reaction (Bjornstrom *et al*., 2004). Nanosilica are small spherical particles of amorphous SiO_2 with sizes ranging from 1nm-500nm. There has been some debate as to whether nanosilica particles are pozzolanic materials or only seeding agents for the hydration process when added to cement pastes (Bjornstromet *et al.*, 2004). Although studies on the interaction between the Portland cement and nanosilica have been carried out (Kawashima *et al*., 2013; Hou *et al.*, 2012; Sato and Beaudoin, 2011; Bjornstrom *et al*., 2004; Raki *et al.*, 2010; Tregger *et al.*, 2010; Sobolev *et al.*, 2009), few studies have considered the interactions with the cementitious materials such as fly ash and microsilica when Portland cement has been used to form a blended cement.

In recent years there has been a real push to lower the carbon footprint of the construction sector therefore less use of Portland cement has been highly encouraged. Fly ash is a pozzolanic material widely used to produce low carbon embodied cement combinations where it can account for up to 50% by mass of the cementitious constituents.

The aim of this work was to evaluate the effects of silica nanoparticles on the calcium silicate hydrates gel network and on the microstructure of the hardened quaternary and quinary cement low Portland cement to fly ash ratio combinations. The C-S-H microstructure morphology was investigated using scanning electron microscopy (SEM) and the Ca/Si ratio was monitored via energy dispersive X-ray microanalyses. Fourier transform infrared was carried out in order to map crystalline and amorphous phases present on the hardened cement pastes. The transmission electron microscopy (TEM) was used to assess the nanosilica particle size and morphology.

EXPERIMENTAL PROCEDURE

Materials

The materials used were a Portland limestone cement, CEMII/A-L42.5, with a limestone content of 14% to which was added additional limestone conforming to EN 197-1. Fly ash conforming to EN 450. Microsilica was provided in an undensified dry form conforming to EN 13263. Two types of nanosilica were used. The first type was an aqueous suspension containing about 30% by mass of nanosilica particles referred as nanosilica-A. The second type was a superplasticiser admixture enhanced with nanosilica reported as 15% by mass of nanoparticles in suspension (nanosilica-B).

To identify the silica nanoparticles present in the suspensions transmission electron microscopy (TEM) was performed. Sample preparation was carried out by diluting 10 µL of the nanosilica suspension in 100 mL of water. At the same time grids were left in an ozone bath for 5 minutes in order to improve the adhesion of samples, after that a drop of the diluted suspensions was dripped on the grids and allowed to dry inside the fume cupboard. Samples were allowed to dry under vacuum for 24h before the TEM analysis. Figure 1 shows nanosilica-A particles with sizes ranging from 8 nm to 50 nm in diameter. EDX was also performed giving the following elemental composition (atomic%): 52.7% of oxygen, 19.5% of silicon, 14.5% of carbon, 12.0% of copper, 0.4% of magnesium, 0.3% of titanium, 0.2% of aluminium, 0.2% of calcium and 0.2% of iron. Although the same testing was performed for nanosilica-B, it was not possible to identify the nanoparticles since they were masked by the superplasticiser present in the suspension. Nanosilica suspensions were also analysed via Fourier transform infrared (FTIR), as shown in Figure 2.

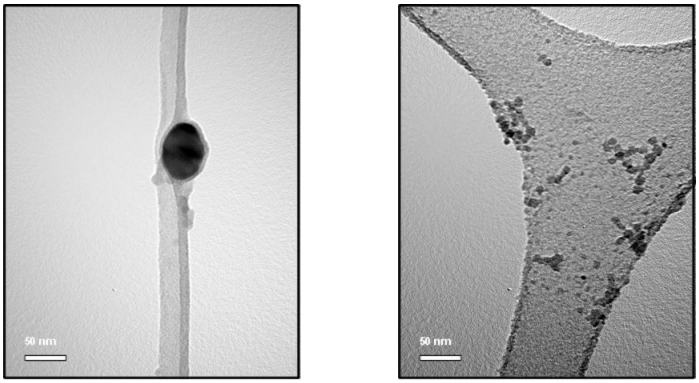

a) b)

Figure 1. - Morphology of nanosilica-A: a) silica nanoparticle of approximately 50nm in diameter and b) Silica nanoparticles of approximately 8nm in diameter.

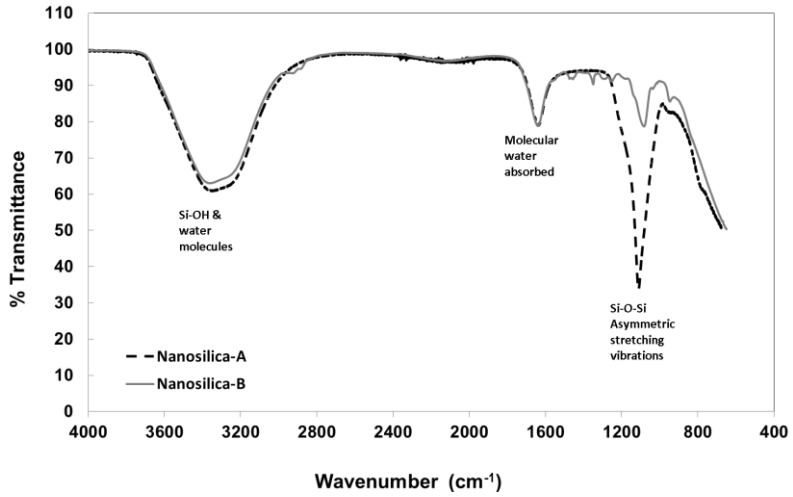

Figure 2. – FTIR fingerprint of nanosilica-A and nanosilica-B suspensions.

Mix design

The mixes proportions of the pastes used are given in Table 1. Pastes were prepared with 43% by mass of Portland cement and 37% by mass of fly ash. The control also contained 20% of limestone by mass. Consisting of net present in CEMII/A-L and the additional limestone added. Microsilica and nanosilica addition were accounted for by the replacement of the limestone content. Paste N-0.5A and N-0.5B were made with nanosilica A and nanosilica B respectively. Paste MN-0.5A was made with a combination of nanosilica A and microsilica. Pastes were prepared using an automatic dual shaft mixer with a speeding rate of 1150 rpm. All dry constituents were pre-mixed for 60 seconds. The liquid phases, water and nanosilica suspension, were added to obtain a water to binder ratio of 0.3 and mixed for further 3 minutes. In the first 24 hours pastes were allowed to hydrate in dry sealed conditions at room temperature. From the second day onwards pastes were cured in water at 20°C.

Table 1- Mix proportions

Mix Proportions - percentage by mass of cementitious material

Paste	PC	LS	FA	$mSiO_2$	$nSiO_2$ solids	W/C	water addition (gr)
C-N0	43	20	37	0	0	0.3	30
N0.5-A	43	19.5	37	0	0.5	0.3	28.8
N0.5-B	43	19.5	37	0	0.5	0.3	28.2
MN0.5-A	43	14	37	5.5	0.5	0.3	28.8

A refers to nanosilica-A and B refers to nanosilica-B.

Arrest of Hydration

To investigate the hydrate gel network microstructure up to 28 days it was necessary to arrest the hydration. Detailed comparisons of hydration arrest of hardened cement pastes have been carried out and they have suggested that different methodologies should be employed for different microstructural analyses (Zhang, 2011; Collier 2008). Therefore two procedures were employed for the arrest of hydration in this work: oven drying and solvent exchange. The oven dry methodology allowed chemical composition investigation, study of phase transformation and crystalline and amorphous phase identification. This methodology was employed in the infrared spectroscopy analysis. In this method samples were broken in small solids and placed in glass containers. Next, samples were placed in a desiccator prepared with NaOH beads. Sodium hydroxide beads were sited on the bottom of the desiccator in order to absorb CO_2 once samples were in the oven, to avoid or minimise carbonation. Desiccator and samples were placed in an oven at 60 °C for 24 hours. In the following day samples were grinded and sieved in a 125 µm mesh sieve. Sodium hydroxide beads were replaced and sieved samples were placed inside the desiccator for another 24 hours in the oven, totalising 48 hours for the procedure to be completed. After this procedure samples presented a stable mass, therefore samples had their mass readings taken before and after they were laid into the oven.

The solvent exchange method allowed samples to be prepared for physical microstructural properties investigation such as morphology and porosity. Scanning electron microscopy and transmission electron microscopy tests were carried out. In this methodology the solvent used was isopropanol, as it was considered to be less aggressive to the microstructure (Zhang, 2011). Samples were broken into small solids and bathed in isopropanol for 24 hours inside a fume cupboard, the solvent to solids ratio was 10:1. After 24 hours, solvent was discarded and samples were vacuum dried in the desiccator for another 24 hours, totalising 48 hours for the procedure to be completed. After this procedure samples presented a stable mass, therefore samples had their mass readings taken before soaking in isopropanol and before and after they went into the desiccator.

Fourier transform infrared (FTIR)

The network of the C-S-H gel is very complex and small changes in the calcium to silicon atomic ratio (Ca/Si ratio) give way to different molecular structures. FT-IR spectroscopy is a powerful technique for identifying silicon derived network. FT-IR is also capable of mapping

amorphous as well as crystalline phases, which in turn is very useful for the investigation of hardened cement based materials.

Tests were performed using a PerkinElmer Frontier Spectrometer and the associated Spectrum software. The technique utilised was attenuated total reflectance (ATR). FTIR spectra were collected with a 0.5 cm^{-1} resolution. Usually 10 scans were accumulated for each spectrum in a frequency range of 600 cm^{-1} – 4000 cm^{-1}. FTIR was carried out for samples after 1, 7 and 28 days.

Scanning electron microscope (SEM)

A suite of SEM analyses was carried out for all samples at the ages of 1, 7 and 28 days. A backscattered electron (BSE) detector and the energy dispersive X-ray microanalysis (EDX) were used to map and detect the distribution of elements in the hardened cement paste at ages of 1, 7 and 28 days for all samples. The fracture samples were less than 1 μm rough (similar to polish cross-section samples) providing enough contrast for the phases to be observed. Two types of SEM equipment were used. The BSE-EDX equipment used was a Jeol 6480 LV. Secondary imaging was generated using a Jeol JSM 6301F field emission scanning electron microscope (FESEM).

RESULTS AND DISCUSSION

The hardened pastes presented several mid-IR frequency regions, described as follows:

Water and hydroxide bands

The spectral range of 4000 cm^{-1} to 2800 cm^{-1} comprises the vibrations associated with water and calcium hydroxide (Trezza, 2007, Hidalgo *et al*., 2006; Lenza and Vasconcelos, 2001). Figure 3a shows the spectra for the control paste containing PC, FA and LS (C-N0). It can be observed that the band assigned to Ca-OH bonds at about 3644 cm^{-1} is present in the spectra of all pastes, in which a slight decrease in intensity can be seen as it ages. The band assigned to stretching vibrations of O-H groups in hydroxyls, silanol groups and hydrogen bonded to each other (2800 – 3600 cm^{-1}) oscillate across the ages. The peak height ratio between the O-H groups (2800 – 3600 cm^{-1}) and the band assigned to Si-OH in polymeric unit of SiO_4^{4-} (around 1000 cm^{-1}) revealed an increased from day 1 to 7 (0.30 to 0.43 respectively). Whereas for day 28 the peak height ratio was of 0.28, showing a decrease in intensity of the band related to free water. A possible explanation for this phenomenon could be that around the age of 7 days pozzolanic reactions, led by the fly ash, were likely to be taking place. The drop of the peak height ratio after 28 days could be an indication that more water became coordinate to form C-S-H gel.

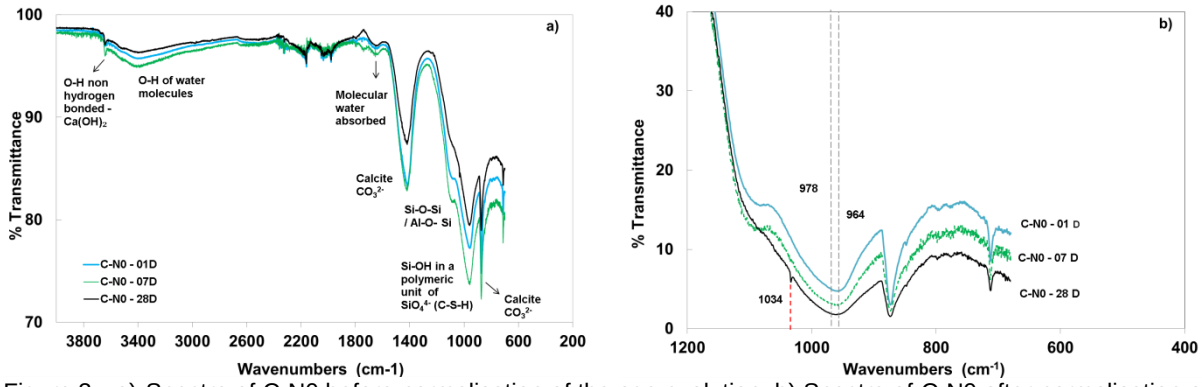

Figure 3 - a) Spectra of C-N0 before normalisation of the age evolution. b) Spectra of C-N0 after normalisation of the age evolution.

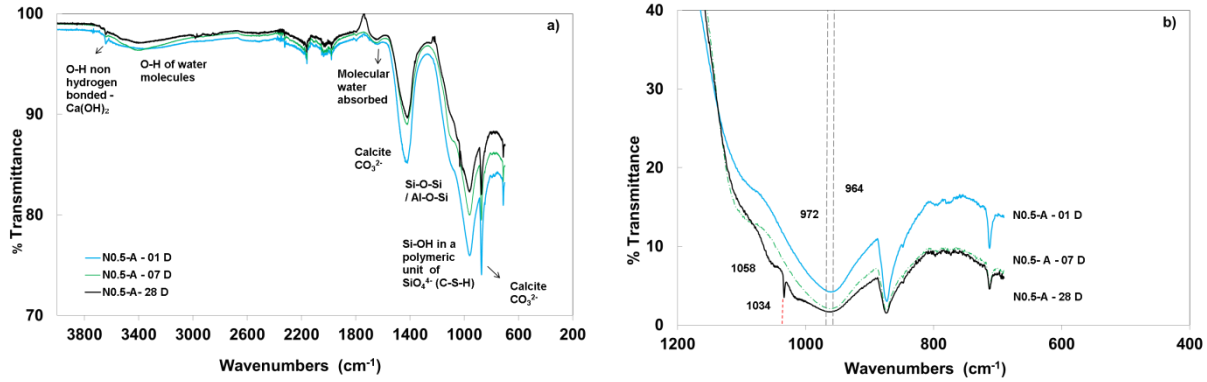

Figure 4 - a) Spectra of N0.5-A before normalisation of the age evolution. b) Spectra of N0.5-A after normalisation of the age evolution.

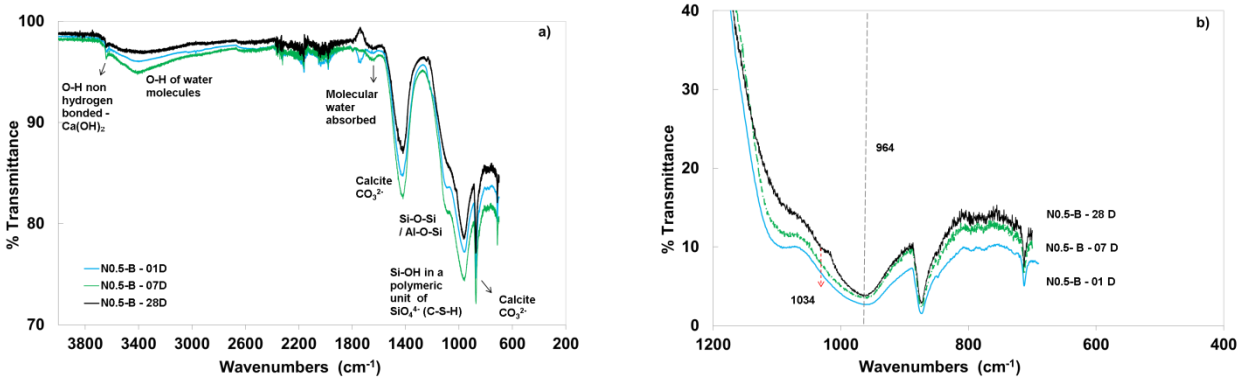

Figure 5 - a) Spectra of N0.5-B before normalisation of the age evolution. b) Spectra of N0.5-B after normalisation of the age evolution

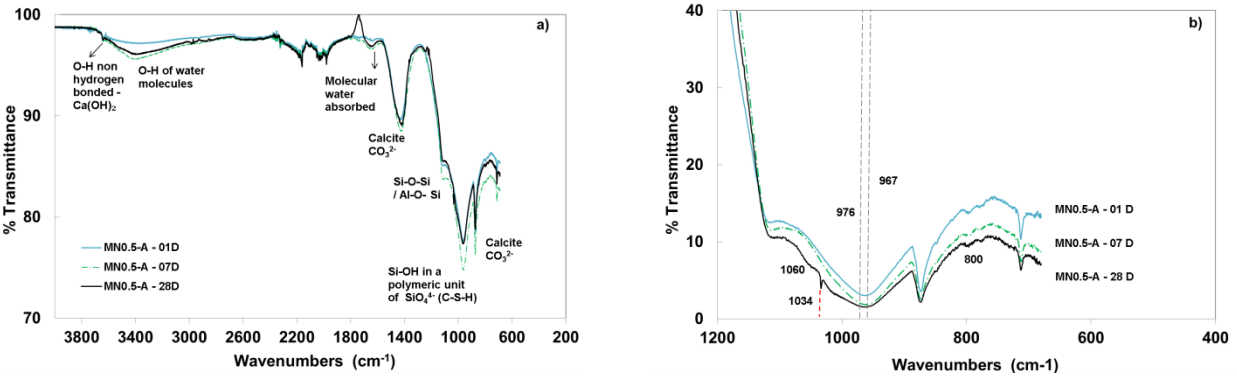

Figure 6 - a) Spectra of MN0.5-A before normalisation of the age evolution. b) Spectra of MN0.5-A after normalisation of the age evolution.

Nanosilica particles are expected to provide early-age strength gain due to the high reactivity between the nanosilica and cement paste as they accelerate the C-S-H network formation. They are also expected to react within the first hours after addition to the paste and provide sites for the condensation of SiO_4 monomers as of the clinker phase dissolution, in the formation of the C-S-H network (Bjornstrom *et al*., 2004). However in this work the two types of nanosilica (A and B) showed different behaviours.

Figure 4a and 6a depict the spectra for N0.5-A and MN0.5-A at ages of 1, 7, and 28 days respectively. Both N0.5-A and MN0.5-A showed the peak ratio between the range associated with O-H of water molecules (2800-3600 cm^{-1}) and the range associated with C-S-H gel (around 1000 cm^{-1}) to be smaller than C-N0 at 1 day (0.19, 0.16 and 0.30 respectively). This could be due to the fact that fly ash volume is much higher than the nanosilica volume resulting in a delay of the effect of the nanosilica particles on hydration. It could also be associated with the high specific surface area of the nanosilica, which reacts more readily with water.

At 7 days N0.5-A and MN0.5-A containing Nanosilica-A showed a decrease in intensity for the peak assigned to calcium hydroxide (3644 cm^{-1}). As for C-N0, this band (3644 cm^{-1}) presented a much sharper peak at the age of 7 days. The decrease associated to this band accounts for the participation of the Ca^{2+} in the network of the C-S-H gel. Showing that between 1 and 7 days the pozzolanic reaction of the nanosilica-A particles have started and the provision of nucleation sites may also have triggered the hydration of the fly ash..

From Figure 5a, it can be seen that for N0.5-B the first signs of pozzolanic reaction started to show after the age of 7 days. Before that the band ascribed to Ca-OH bonds at about 3644 cm^{-1} presented almost the same shape and intensity as observed for the control (C-N0). N0.5-B sample, at the age of 28 days, showed for the band of CaOH linkages lower intensity when compared to 1 and 7 day pastes. It could indicate that in the presence of fly ash nanosilica-B starts to take part in the hydration process later on.

The differences in behaviour of the nanosilica-B can be due to: (i) surfactant-treated silica nanoparticles (nanosilica-B) could balance the speed of their interaction with cement therefore delaying the process of a second hydration (pozzolanic reaction). (ii) the high volume of fly ash present in the cement paste (37% by mass) could be aggravating this delay. When fly ash and microsilica particles are added together in the same mixture, fly ash particles can delay the accelerating effect of microsilica (Langan *et al*., 2002) in which by analogy is very likely to show the same effect on nanosilica. Negative aspects can be accounted to surfactant treated nanosilica which could compromise early-age strength gain (Pengkun Hou, 2012) and setting time as observed in this work for pastes containing nanosilica-B, which took over a day to fully set.

Silica in the C-S-H network

In the region of 1260 cm^{-1} to 1000 cm^{-1} bands are associated with asymmetric stretching vibrations of Si-O-Si (Lopez *et al*., 2008; Hidalgo *et al*., 2006; Bjornstrom *et al*., 2004; Lenza and Vasconcelos, 2001; Ping Yu *et al*., 1999). As the hydration progresses, the bands around 1000 cm^{-1} gradually broaden to comprise vibrations of higher frequencies (up to 1260 cm^{-1}). As a result of the hydration process and formation of C-S-H gel networking this

shift (from lower to higher vibrational frequencies) of the Si-O stretching vibration can be identified as a strong indication of more complex degree of polymerisation (Bjornstrom *et al*., 2004). On the other hand, when this shift is observed at lower vibration frequencies (< 960 cm^{-1}) and an increase of the Ca/Si ratio is also observed it can be associated to depolymerisation of the silica network in the C-S-H. (Ping Yu *et al*., 1999)

In order to eliminate the path length variation and to reduce the differences between each single measurement, normalisation was carried out. The chosen band was in relation to the most intense water band (3422 cm^{-1}) (Mansur *et al*., 2008; Davis and Manuer, 2010). Figures 3b, 4b, 5b and 6b show the normalised spectra for the samples C-N0, N0.5-B, N0.5-A, MN0.5-A respectively.

In a silicate network various forms of Si-O bonding can be observed. The basic tetrahedral unit $(SiO4)^{4-}$ is denoted as (Q^0) which is due to isolated silicate tetrahedra in the crystal structure of unhydrated C_3S. The subscript designates the number of $(SiO_4)^{4-}$ attached to the central tetrahedral unit. Q^1 site represents a dimer, where Q^2 site accounts for silicon atoms in a polymeric chain of tetrahedral silica. Q^1 is assigned to the end of the chain while Q^2 is the bridging tetrahedra in the middle of the silicate chain. Q^3 and Q^4 account for silicon centres where much more complex structures are formed (Beaudoin *et al*., 2009; Richardson, 2008; MacLaren and White, 2003).

Those vibrational modes can be detected and differentiated in the IR spectroscope. The more polymerised a C-S-H network is, the higher is the vibrational frequencies of the silicate structures. According to Yu *et al*. (1999) and Bjornstrom *et al*. (2004) in a C-S-H gel network Q^1 accounts for vibrational frequencies at around 811 cm^{-1}. Q^2 vibrational modes are identified by a well defined peak at around 980 cm^{-1} and by a shoulder at around 1060 cm^{-1}.. The FTIR spectra showed the presence of the Q^1 and Q^2 vibrational modes.. It has been reported in previous work (Yu *et al*., 1999) that the shoulder at around 1060 cm^{-1} and the band at about 980 cm^{-1} are associated to Si-O stretching vibrations at Q^2 sites. In this work the presence of this shoulder was detected for the N0.5-A and MN0.5-A samples at around 1058 cm^{-1}

The normalised spectra for C-N0 N0.5-A, MN0.5-A at 28 days (Figures 3b, 4b, 6b respectively) display more clearly the appearance of a sharp peak at about 1034 cm^{-1}. This band can be associated with Si-O stretching vibration, suggesting more organised segments of the SiO_4 being formed in the C-S-H gel network. However there was not enough evidence to associate this particular peak with a specific degree of polymerisation. This sharp peak was detected on C-N0 (Figure 3b), MN0.5-A (Figure 6b) and N0.5-A (Figure 4b) at 28 days increasing in intensity respectively.

Free silanol groups on the surface of the C-S-H gel

Spectral interval of 900 cm^{-1} - 980 cm^{-1} is assigned to Si-O stretching vibration (Trezza, 2007; Bjornstrom, 2004; Lenza and Vascocelos, 2001; Ping Yu *et al*., 1999); It can be observed for the normalised age evolution of all the pastes C-N0, N0.5-A, N0.5-B MN0.5-A (Figures 3b, 4b, 5b, and 6b respectively) that there is a shift of the main band assigned to C-S-H at around 964 cm^{-1} at 1 day when compared to 7 and 28 days. For C-N0, N0.5-A and MN0.5-A (Figures 3b, 4b, and 6b) this shift occurs towards vibrations of higher frequencies

and it is also possible to see the shoulder at around 1060 cm^{-1} associated with Q^2 (bridging tetraedra in a silicate chain) vibrational modes, as mentioned before.

Alumino-silicate bonding and carbonates

The band 1034 cm^{-1} can also be associated with alumino-silicate bonding (Sakulich 2009; Ylmén *et al*., 2009; Trezza, 2007; Hidalgo *et al*., 2006; Katti 2001*)* indicating that by the age of 28 days fly ash has started to react. This phase appeared to increase in presence of microsilica and nanosilica especially when nanosilica-A was added to the paste*.* The similarity of the C-S-H network in presence of nanosilica and clay microstructure assembly has also been discussed in previous works (Bjornstrom *et al*. 2004). It has been reported that clinker phase releases monomeric silica which will give form to polymeric structures such as dimers andsilicate chains. Ca^{2+} ions and water molecules act as stabilisers in layered clay minerals structures. The C-S-H gel has an analogue structural configuration in which can be expected a considerable number of inter-layer hydrogen bonding between Si-OH groups and OH^- coordinated with Ca^{2+} ions. Incomplete hydration process segregates $Ca(OH)_2$. It is possible that the formation of $Ca(OH)_2$ is due to water deficiency. By protecting the cement paste from dehydration, the precipitation of calcium hydroxide becomes subdued therefore the Ca^{2+} ions can then take part in the formation of the C-S-H clay-like structure (Bjornstrom *et al*. 2004). Figure 9c shows C-S-H microstructure developed N0.5-A and MN0.5-A where the resemblance with clay structure can be observed. The seeding effect of the nanosilica-A and microsilica combination can be seen taking place in the $Ca(OH)_2$ crystals. Previous work (Weerdt *et al*. 2011a) also suggests that limestone does not only act as filler but also increases the volume of hydrates. Which in the presence of fly ash more aluminates are formed thereby lowering the sulfate/aluminate ratio.

The normalised spectra for the age evolution of N0.5-B (Fig. 5b) at 1, 7 and 28 days show for the pastes at 1 and 7 days the presence of a shoulder at around 1100 cm^{-1}. However, for N0.5-B 28 days this band is broader and the disappearance of the 1100 cm^{-1} shoulder can be observed. According to previous study (Bjornstrom *et al*., 2004), the inclusion of the 1100 cm^{-1} shoulder suggests that the C-S-H hydration is progressing (incorporation of nanosilica particles) being also an indicative of more complex silicate networking and a higher degree of connectivity of SiO_4^- in the C-S-H network.

The bands at around 1440 cm-1, 875 cm-1 and 713 cm-1 are attributed to CO_3^{-2} vibrational groups due to the presence of limestone ($CaCO_3$) of up to 20% in the mix formulations and not due to carbonation of the pastes. On the other hand there is not enough evidence in this work to say that the apparent decrease in the peaks associated with limestone, as hydration progresses, are due to the reaction of calcite with aluminate to form carboxyaluminates.

Sulfate bands

Sulfate adsorption bands are also found in this area (1200 cm^{-1}-1100 cm^{-1}) due to the ettringite SO_4^{2-} vibration group which are very difficult to identify by the FTIR technique alone as they overlap with silicate network. According to previous works (Weerdt *et al*. 2011a and Weerdt *et al*. 2011b) limestone affects blended Portland fly ash cement systems positively. Limestone interacts with hydration products formed, preventing the decomposition of ettringite to monusulfate giving way to phases such as hemicarboaluminate.This region is also associated with the microsilica and nanosilica main band (1120 cm^{-1}) and to the main

band assigned to the fly ash at around 1085 cm^{-1} (Ylmén et al., 2009 and Calvo et al., 2013). The shoulder at around 1100 cm^{-1} present in all samples tend to disappear at the age of 28 days, given way to a broader band, which can be directly associated with the C-S-H absorption bands.

Ca/Si ratio

According to previous studies (Skinner, 2010; Beaudoin *et al.*, 2009; Yu, 1999; Nonat, 1998) there is a correlation between the degree of silica polymerisation in the formation of the C-S-H network and the Ca/Si ratio. It has been reported that a decrease in the Ca/Si ratio is correlated with an increase in the mean length of silicate chains as well as the distance between the C-S-H layers which is one of the most important changes in the calcium silica hydrates (Beaudoin *et al..* 2009). The polymerisation (number of silicate tetraedral in a chain) of C-S-H is dependent on its compositional Ca/Si ratio. The silicon chain length increase can be directly correlated with the decrease in Ca/Si ratios as relatively low Ca/Si ratios approaching 1.0 are likely to present more silicate dimers than monomers. Addition of fly ash and microsilica to Portland cement results in formation of additional C-S-H gel, which could possess a low Ca/Si ratio. This C-S-H according to previous studies has a calcium silicate hydrate network more polymerised with different characteristics, one of them being assigned to enhancement in durability (Raki *et al.*, 2010; Beaudoin *et al.*, 2009).

Table 2 shows the Ca/Si ratio assessed in the C-S-H gel in the hardened cement paste, for all samples, at the age of 28 days, obtained by EDX. Sample C-N0 had the highest Ca/Si atomic ratio (2.3). From the FTIR spectra (Figure 3a) one can observe that the band associated with $Ca(OH)_2$ is less intense at the age of 28 days suggesting that part of the calcium hydroxide produced during the hydration process has partially been utilised in the pozzolanic reactions lead by the fly ash. Although the literature suggests that the fly ash could deliver low Ca/Si ratios it was not observed for this sample.

It can be observed that the Ca/Si ratio at 28 days is lower for N0.5-B than that detected for C-N0. This could be because the C-S-H gel is denser but due to the surfactant present in nanosilica-B admixture, there may also be a delay in the cement hydration. Therefore at this stage, the C-S-H gel formation is incomplete rather than silica rich (low Ca/Si ratio), characteristic of a more polymerised C-S-H network. Further investigations on the effect of nanosilica-B t were beyond the scope of this work.

N0.5-A presented lower Ca/Si ratio (1.8) when compared to the reference sample (C-N0). The FITR spectra (4a) show a less sharp peak in the region of $Ca(OH)_2$ (3644 cm^{-1}) suggesting the nanosilica-A is acting as a seeding agent to form C-S-H. As the Ca/Si atomic ratio is lower than observed when fly ash is acting alone.

MN0.5-A presented the lowest Ca/Si atomic ratio among all the samples, specially when compared to the reference sample C-N0, indicating that microsilica and nanosilica-A work well together and the accelerating behaviour of the microsilica apparently helped to even lower the Ca/Si ratio, where changes in microstructure can be observed. The effect of supplementary cementitious on lowering the Ca/Si ratio of the C-S-H gels has also been reported by other researchers (Lothenbach *et al*. 2011)

Table 2- Ca/Si atomic ratio (%) for 28 day-old samples.

Paste	Ca/Si Atomic ratio (%)
	28 days
C-N0	2.3
N0.5-A	1.8
N0.5-B	1.8
MN0.5-A	1.2

Microstructure

A suite of SEM-EDX analyses was carried out at 1, 7 and 28 days. Figures 4 to 6 show SEM micrographs in which the microstructure of C-N0, N0.5-A, MN0.5-A and N0.5-B at 28 days can be observed. Figure 7 shows that at low magnifications, pastes have similar morphology except for N0.5-A which has patches of what appears to be denser cement paste. The pozzolanic reaction of the fly ash particles can be observed in Figure 8 where they are covered in what appears to be C-S-H gel and other hydration products. Furthermore N0.5-B (Figure 8d) shows a fly ash particle burst and the nucleation of C-S-H gel taking place. Figure 9 depicts the morphology for the four pastes in which hydration products of fibrilar morphology (needle-like) and C-S-H gel can be found in all pastes. MN0.5-A (Figure 9c) shows a distinct morphology, a foil-like structure, being developed on a CH crystal. This could be an indication that nanosilica-A together with microsilica particles could be acting as catalyst for the hydration process as well as a seeding agent for the nucleation of the C-S-H gel (honeycomb structure on a CH crystal). This change in morphology, from needle- to foil-like structures has also been observed by other researchers (Scrivener and Nonat, 2011; Richardson, 1999) and has been partially attributed to a refinement in porosity when supplementary cementitious materials are used.

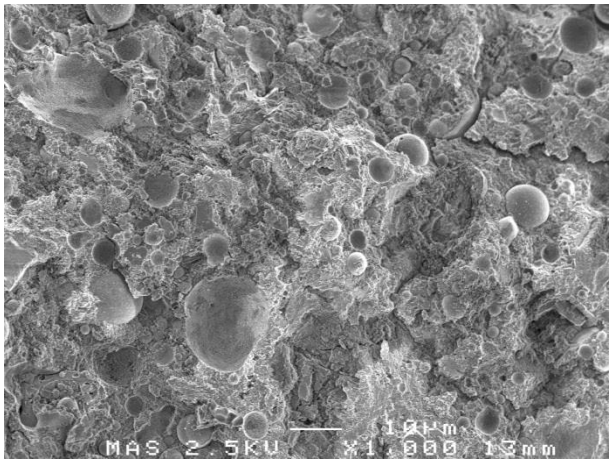

a) C-N0
(43%pc/20%ls/37%fa)

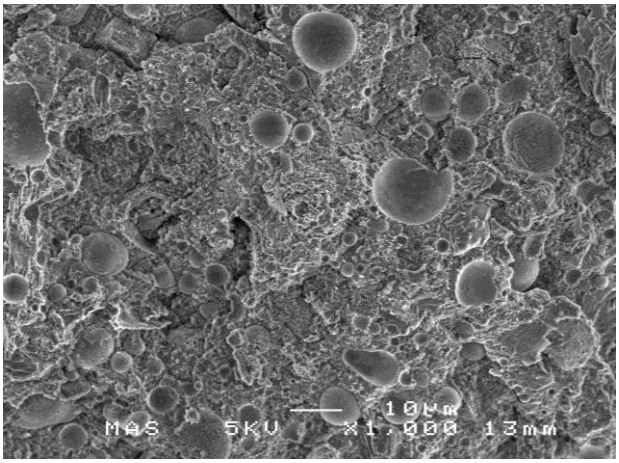

b) N0.5-A
(43%pc/19.5%ls/37%fa0.5%NS)

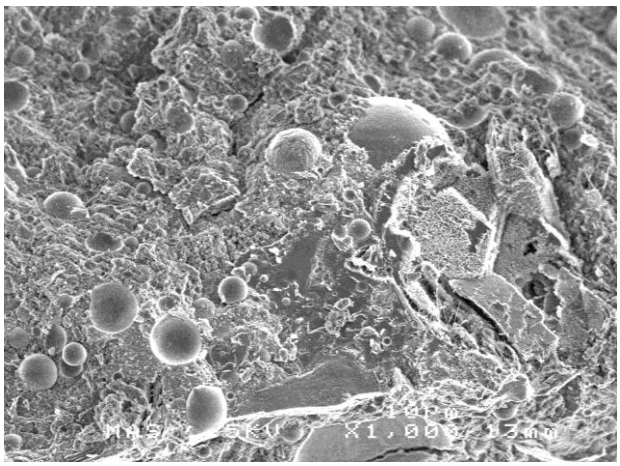

c) MN0.5-A
(43%pc/19.5%ls/37%fa/0.5%ns/5.5%ms)

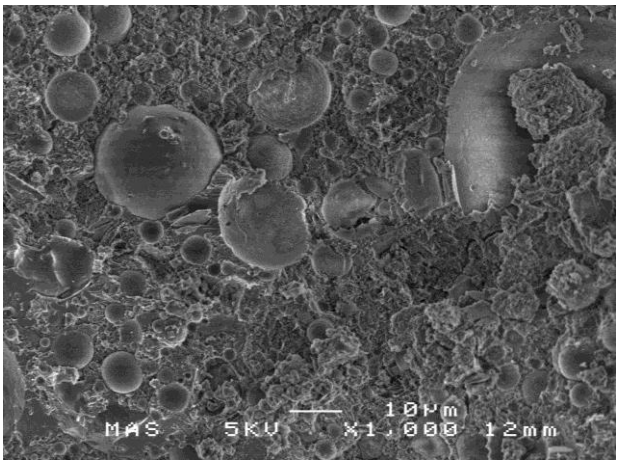

d) N0.5-B
(43%pc/19.5%ls/37%fa0.5%NS)

Figure 7 - SEM micrographs at 28 days at low magnification.

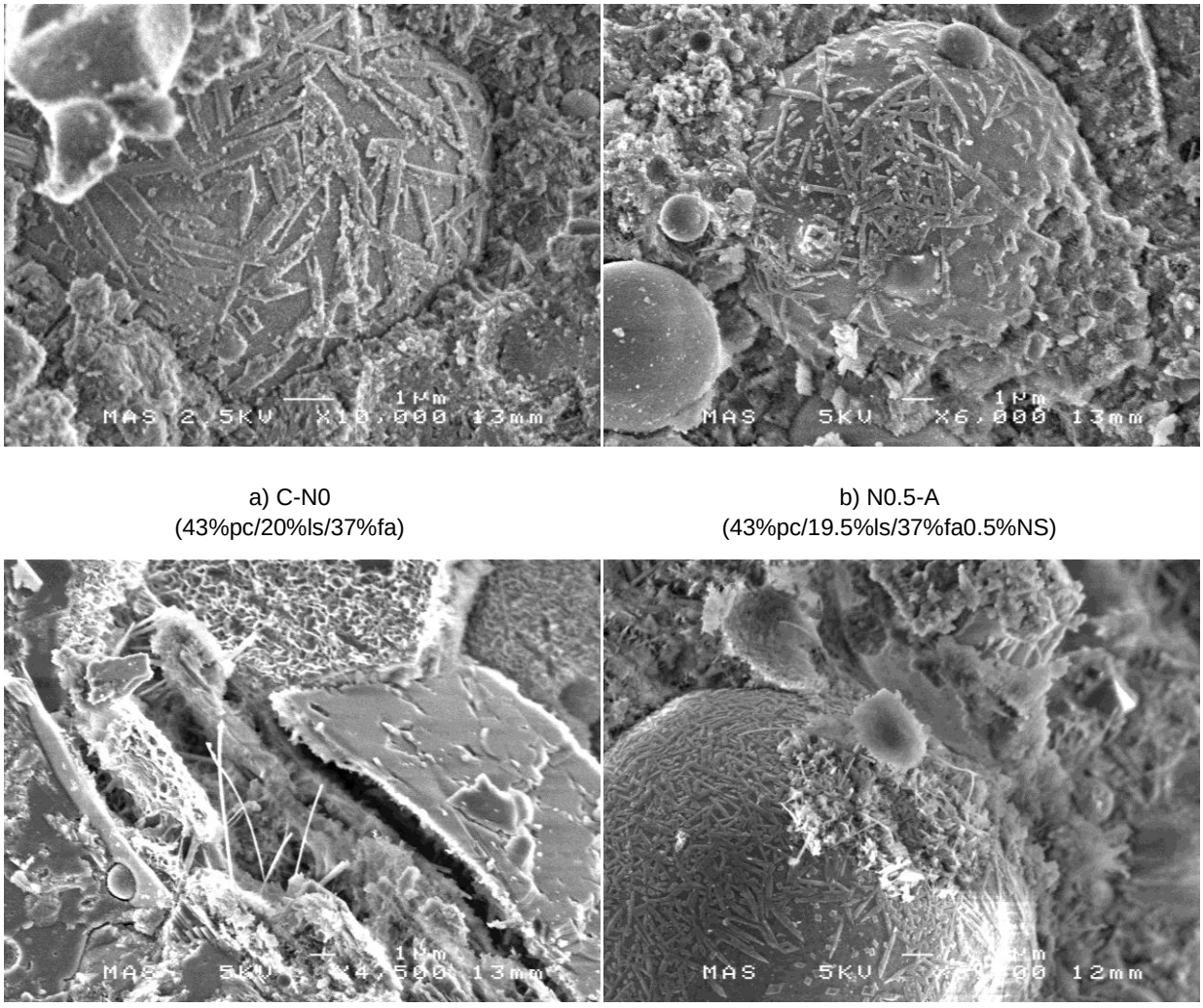

a) C-N0
(43%pc/20%ls/37%fa)

b) N0.5-A
(43%pc/19.5%ls/37%fa0.5%NS)

c) MN0.5-A
(43%pc/19.5%ls/37%fa/0.5%ns/5.5%ms)

d) N0.5-B
(43%pc/19.5%ls/37%fa0.5%NS)

Figure 8 - SEM micrographs of 28 days showing C-S-H nucleation.

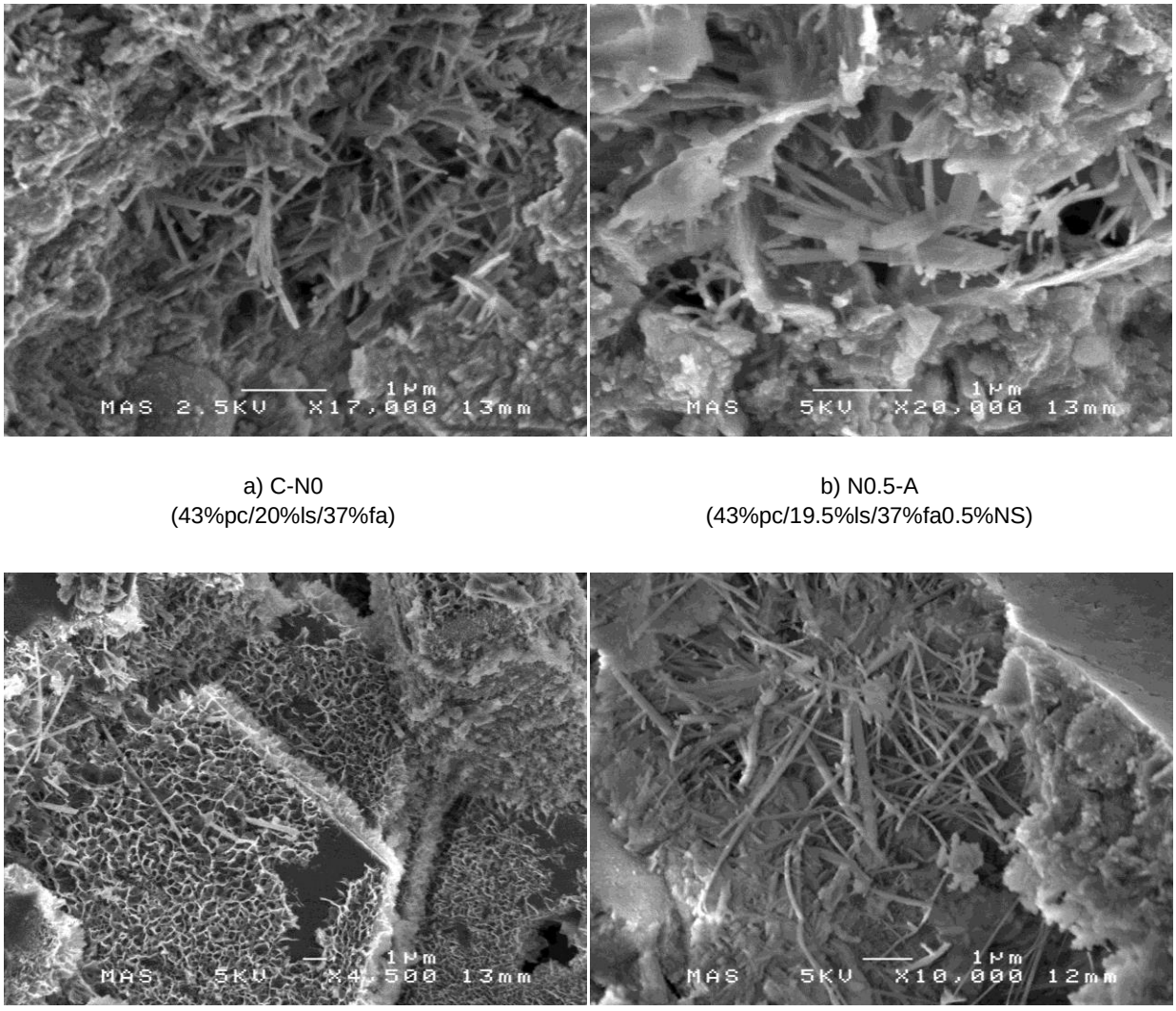

a) C-N0
(43%pc/20%ls/37%fa)

b) N0.5-A
(43%pc/19.5%ls/37%fa0.5%NS)

c) MN0.5-A
(43%pc/19.5%ls/37%fa/0.5%ns/5.5%ms)

d) N0.5-B
(43%pc/19.5%ls/37%fa0.5%NS)

Figure 9 - SEM micrographs of 28 days showing C-S-H nucleation and differences in morphology.

It is important to notice that as a result of the low Ca/Si ratio produced by nanosilica it could create denser C-S-H gels, which can act as ion penetration barriers. These dense calcium silicate gels can be formed around unreacted fly ash particles creating unhydrated pockets, impeding homogeneous hydration of the cement paste (Kawashima *et al*., 2013 and Wang *et al*., 2012). There is also a possibility for the fly ash to suffer calcium hydroxide starvation in cases where the nanosilica particles react too quickly. In this work at the age of 28 days it was not possible to identify whether the unhydrated fly ash particles were surrounded by denser C-S-H or not (Figures 7, 8, and 9). On the other hand, the presence of a band related to $Ca(OH)_2$ (Figure 4a, 5a, 6a) could still be observed for all samples containing nanosilica at the age of 28 days, indicating that pozzolanic reactions can still take place after the age of 28 days.

CONCLUSIONS

Portland cement, fly ash and limestone combinations were investigated in presence of microsilica and nanosilica giving way to ternary, quaternary and quinary cement mixes, with an objective to investigate the role of the nanosilica in the hydration process and morphology. Complementary techniques were employed: ATR-FTIR, SEM and EDX in order to improve the understanding of the hydration products especially the C-S-H gel network. The findings of this investigation can be summarised as follows:

- Addition of nanosilica increased pozzolanic activity in the quaternary (fly ash) and quinary (fly ash and microsilica) systems.
- In pozzolanic reactions fly ash and nanosilica are competitors feeding from the calcium hydroxide crystal sheets produced during the cement hydration, to form additional calcium silicate hydrates. Nanosilica-A particles used in this work varied from 8 nm to 50 nm in size whereas fly ash particles vary from 0.5 µm to 300 µm. Two situations can be drawn when both materials are present in a cement paste,: (i) the nanoparticles being smaller could react faster than the fly ash particles, therefore leaving less CH for the fly ash to promote more pozzolanic reactions later on and (ii) due to the large amount of fly ash (37%) in comparison to the nanosilica addition (0.5%) it is possible that the slower reaction the fly ash is delaying the effect of the nanosilica.
- Ca/Si ratios reduced as nanosilica was added. This can be accounted for by two routes: seeding effect of the nanosilica in the formation of the C-S-H network and/or by the calcium hydroxide, product of the hydration, donated atoms of calcium to form the C-S-H gel, which in turn, derived from a pozzolanic reaction.
- ATR-FTIR is a useful tool to follow structural changes that occur in the C-S-H gel network. At the age of 28 days C-N0, N0.5-A and MN0.5-A presented bands characteristic of bridging silicate tetraedra in a chain, with higher intensities for samples with nanosilica-A, whereas for N0.5-B it was only possible to detect pairs of silicate tetraedral. Higher intensity for the region associated with $Ca(OH)_2$ is observed in the spectrum of the control sample (C-N0) indicating more unreacted calcium hydroxide crystals at 28 days. Lower intensity of the band associated with $Ca(OH)_2$ was observed for the pastes containing nanosilica which indicates that the seeding effect of the nanoparticles in the C-S-H formation is taking place.
- Results obtained by the EDX confirmed that the MN0.5-A paste shows a higher degree of polymerisation in the C-S-H network, presenting a low Ca/Si atomic ratio (1.2) characteristic of denser C-S-H gel opposed to the C-N0 sample (Ca/Si of 2.3). The micrographs also showed a more complex arrangement of the microstructure, honeycomb-like structure, for the MN0.5-A sample (Figure 9c).
- Results suggest that the addition of nanosilica-A in Portland cement-fly-ash systems modifies the network of the C-S-H leading to a more complex arrangement of the microstructure which is silicon rich. These effects are more pronounced in mix combinations where microsilica is also present.

Further studies should be carried out in order to investigate the homogeneity of the nanosilica effect in the microstructure.

ACKNOWLEDGMENTS

Authors would like to acknowledge the European Commission funding – FIBCEM project, grant Number (262954) and all partners are thanked for their input and for supplying materials.

REFERENCES

Beaudoin JJ, Raki L, Alizadeh R (2009) A ^{29}Si MAS NMR study of modified C–S–H nanostructures. *Journal of Cement and Concrete Composites Elsevier* **31(8)**: 585–590.

Bentz DP, Sato T , Varga I , Weiss W J (2012) Fine limestone additions to regulate setting in high volume fly ash mixtures. *Journal of Cement and Concrete Composites Elsevier* **34 (1):** 11–17.

Bjornstrom J, Martinelli A, Matic A, Borjesson L, Panas I (2004) Accelerating effects of colloidal nano-silica for beneficial calcium–silicate–hydrate formation in cement. *Journal of Chemical Physics Letters Elsevier* **392(1-3)**: 242–248.

Calvo JLG, Moreno MS, Alonso MCA, Hidalgo AL, Olmo JG (2013) Study of the Microstructure Evolution of Low-pH Cements Based on Ordinary Portland Cement (OPC) by Mid- and Near-Infrared Spectroscopy, and Their Influence on Corrosion of Steel Reinforcement. *Materials MDPI* **6(6)**: 2508-2521.

Collier NC, Sharp JH, Milestone NB, Hill J, Godfrey IH (2008**)** The influence of water removal techniques on the composition and microstructure of hardened cement pastes. *Journal of Cement and Concrete Research Elsevier* **38(6)**: 737-744.

Davis R, Mauer LJ (2010) Fourier transform infrared (FT-IR) spectroscopy: A rapid tool for detection and analysis of foodborne pathogenic bacteria. *Current research, technology and education topics in applied microbiology and microbial biotechnology Formatex* **2**:1582-1594.

Hidalgo A, Petit S, Domingo C, Alonso C, Andrade C (2007) Microstructural characterisation of leaching effects in cement pastes due to neutralisation of their alkaline nature. Part I: Portland cement pastes. *Journal of Cement & Concrete Research Elsevier* **37(1)**: 63-70.

Hou P, Wang K, Qian J, Kawashima S, Kong D, Shah SP (2012) Effects of colloidal nanoSiO_2 on fly ash hydration. *Journal of Cement and Concrete Composites Elsevier* **34(10):** 1095–1103.

Katti K, Katti D (2001) Effect of clay-water interactions on swelling in montmorillonite clay. *In 16th Engineering Mechanics Conference*.

Kawashima S, Hou P, Corr DJ, Shah SP (2013) Modification of cement-based materials with nanoparticles. *Journal of Cement and Concrete Composites Elsevier* **36**: 8-15.

Langan BW, Weng K, Ward, MA (2002) Effect of silica fume and fly ash heat of hydration of Portland cement. *Journal of Cement and Concrete Research* Elsevier **32(7)**: 1045-1051.

Lenza RFS, Vasconcelos WL (2001)a Structural evolution of silica sols modified with formamide. *Materials Research Scielo* **4(3)**: 175-179.

Lenza RFS, Vasconcelos WL (2001)b Preparation of silica by sol-gel method using formamide. *Materials Research Scielo* **4(3)**: 189-194.

Lopez AH, Calvo JLG, Olmo JG, Petit S, Alonso MC (2008) Microstructural Evolution of Calcium Aluminate Cements Hydration with Silica Fume and Fly Ash Additions by Scanning Electron Microscopy, and Mid and Near-Infrared Spectroscopy. *Journal of American Ceramic Society Wiley* **91(4)**: 1258-1265.

Lothenbach B, Scrivener K, Hooton RD (2011) Supplementary cementitious materials. *Journal of Cement and Concrete Research*, **41(12)**: 1244-1256.

MacLaren DC, White MA (2003) Cement: Its Chemistry and Properties. *Journal of Chemical Education ACS*, **80(6)**: 623-635.

Mansur HS, Sadahira CM, Souza AN, Mansur AAP (2008) FTIR spectroscopy characterization of poly (vinyl alcohol) hydrogel with different hydrolysis degree and chemically crosslinked with glutaraldehyde. *Journal of Materials Science and Engineering: C* **28(4)**: 539–548.

Nonat A and Lecoq X (1998) Nuclear Magnetic Resonance Spectroscopy of Cement-Based Materials. The structure, stoichiometry and properties of C-S-H prepared by C3S hydration under controlled conditions (Colombet P *et al* (Eds)), Springer, Berlin, DE, pp. 197–207.

Raki L, Beaudoin J, Alizadeh R, Makar J, Sato T (2010) Cement and Concrete Nanoscience and Nanotechnology. *Materials MDPI* **3(2)**: 918-942.

Richardson IG (1999) The nature of C-S-H in hardened cements. *Journal of Cement and Concrete Research* **29(8)**: 1131-1147.

Richardson IG (2008) The calcium silicate hydrates. *Journal of Cement and Concrete Research* **38(2)**: 137-158.

Sakulich AR (2009) Characterisation of Environmental-Friendly Alkali Activated Slag Cements and Building Materials, PhD thesis.

Sato T, Beaudoin JJ (2011) Effect of nano-CaCO3 on hydration of cement containing supplementary cementitious materials. *Journal of Advances in Cement Research ICE* **23(1)**: 33-43.

Scrivener KL, Nonat A (2011) Hydration of cementitious materials, present and future. *Journal of Cement and Concrete Research* **41(7)**: 651-665.

Skinner LB, Chae SR, Benmore CJ, Wenk HR, Monteiro PJM (2010) Nanostructure of Calcium Silicate Hydrates in Cements. *Journal of Physical Review Letters APS* **104(19)**: 195502.

Sobolev K, Flores I, Torres LM, Valdez PL, Zarazua E, Cuellar EL (2009) Engineering of SiO_2 Nanoparticles for Optimal Performance in Nano Cement-Based Materials. *Proceedings of the NICOM3 - Nanotechnology in Construction 3*, pp.139-148.

Tregger N, Pakula M, Shah SP (2010) Influence of Micro- and Nanoclays on Fresh State of Concrete. *Journal of the Transportation Research Board - Nanotechnology in Cement and Concrete* 1, pp. 68-74, http://dx.doi.org/10.3141/2141-12

Trezza MA (2007) Hydration study of ordinary Portland cement in the presence of zinc ions. *Materials Research Scielo* **10(4)**: 331-334.

Wang Q, Feng J, Yan P (2012) The microstructure of 4-year-old hardened cement-fly ash paste. *Construction and Building Materials Elsevier* **29**: 114-119.

Weert KD, Kjellsen KO, Sellevold E, Justnes H (2011)a Synergy between fly ash and limestone powder in ternary cements. *Journal of Cement and Concrete Composites* **33(1)**: 30-38.

Weert KD, Haha MB, Saout GL, *et al*. (2011)b Hydration mechanisms of ternary Portland cements containing limestone powder and fly ash. *Journal of Cement and Concrete Research* **41(3)**: 279-291.

Ylmén R, Jäglid U, Steenari BM, Panas I (2009) Early hydration and setting of Portland cement monitored by IR, SEM and Vicat techniques. *Journal of Cement and Concrete Research Elsevier* **39(5)**: 433-439.

Yu P, Kirkpatrick RJ, Poe B, McMillan PF, Cong X (1999) Structure of calcium silicate hydrate (C-S-H): near-, mid-, and far-infrared spectroscopy. *Journal of American Ceramic Society Wiley* **82(3)**: 742-748.

Zhang J, Scherer GW (2011) Comparison of methods for arresting hydration of cement. *Journal of Cement and Concrete Research Elsevier* **41(10)**: 1024-1036.